

Fundamental plane distances to early-type field galaxies in the South Equatorial Strip

I. The spectroscopic data

K.R. Müller^{1,2}, G. Wegner¹, S. Raychaudhury³, and W. Freudling²

¹ Department of Physics and Astronomy, Dartmouth College, 6127 Wilder Laboratory, Hanover, NH 03755, U.S.A.

² European Southern Observatory and Space Telescope – European Coordinating Facility, Karl Schwarzschild Str. 2, D-85748 Garching bei München, Germany

³ Inter-University Centre for Astronomy and Astrophysics, Ganeshkhind, Pune 411 007, India

Received June 25; accepted September 8, 1999

Abstract. Radial velocities and central velocity dispersions are derived for 238 E/S0 galaxies from medium-resolution spectroscopy. New spectroscopic data have been obtained as part of a study of the Fundamental Plane distances and peculiar motions of early-type galaxies in three selected directions of the South Equatorial Strip, undertaken in order to investigate the reality of large-scale streaming motion; results of this study have been reported in Müller et al. (1998). The new APM South Equatorial Strip Catalog ($-17^{\circ}5 < \delta < +2^{\circ}5$) was used to select the sample of field galaxies in three directions: (1) 15h10 – 16h10; (2) 20h30 – 21h50; (3) 00h10 – 01h30. The spectra obtained have a median S/N per Å of 23, an instrumental resolution (FWHM) of ~ 4 Å, and the spectrograph resolution (dispersion) is ~ 100 km s⁻¹. The Fourier cross-correlation method was used to derive the radial velocities and velocity dispersions. The velocity dispersions have been corrected for the size of the aperture and for the galaxy effective radius. Comparisons of the derived radial velocities with data from the literature show that our values are accurate to 40 km s⁻¹. A comparison with results from Jørgensen et al. (1995) shows that the derived central velocity dispersion have an rms scatter of 0.036 in $\log \sigma$. There is no offset relative to the velocity dispersions of Davies et al. (1987).

Key words: techniques: spectroscopic — galaxies: distances and redshifts — galaxies: elliptical and lenticular, cD — galaxies: fundamental parameters

1. Introduction

The observed total radial velocity of a galaxy (found from the redshift) can be separated into two distinct parts: a cosmological part, from the expansion of the universe, and a peculiar motion associated with the galaxy proper motion. Measurements of galaxy peculiar velocities on large scales reveal the underlying mass density fluctuations, since galaxies will stream towards an overdense region and away from an underdense region.

To determine peculiar motions, a distance-indicator relation has to be used to find redshift-independent distances to galaxies. The Tully-Fisher relation can be used for spiral galaxies. Elliptical galaxies have been found to populate a nearly planar region in the three-dimensional space defined by the central velocity dispersion, the effective (half-luminosity) radius, and the effective surface brightness; this region is called the Fundamental Plane (Lucrey et al. 1991; Jørgensen et al. 1993). The Fundamental Plane (FP) method for distance determination is an improvement on the $D_n - \sigma$ relation. It has a tighter correlation; therefore, a better precision in distances ($\sim 20\%$) can be achieved (Jørgensen et al. 1996; Scodreggio et al. 1997).

Galaxy peculiar velocities are found from a comparison of the distances with the measured redshifts. There is strong observational evidence for the existence of large-scale flows in the local universe, induced by gravity (see Strauss & Willick 1995). The dipole anisotropy of the cosmic microwave background (CMB) radiation provides a natural velocity reference frame for the analysis of galaxy motions. The dipole anisotropy, determined from COBE, implies that the Local Group (LG) moves with respect to the CMB rest frame at 627 ± 22 km s⁻¹ towards $l = 276 \pm 3^\circ$, $b = +30 \pm 3^\circ$ (Kogut et al. 1993). If this

has a kinematic origin then, sufficiently far away, galaxy peculiar velocities should converge to the CMB frame.

Until now, the only studies which have reported measurements of the velocity field as far out as $15\,000\text{ km s}^{-1}$ are those of Lauer & Postman (LP) (1994), using brightest cluster galaxies as distance indicators, and Riess et al. (1995), using Type Ia supernovae. LP checked the convergence of the LG dipole motion to the CMB dipole, with a surprising result: a strong signature of a very large-scale bulk flow was seen, with an amplitude of $689 \pm 178\text{ km s}^{-1}$ in the direction $l = 343^\circ$, $b = +52^\circ$. The LP study implies that the local rest frame fails to converge to the CMB frame, even in regions with radii $\sim 15\,000\text{ km s}^{-1}$. A bulk flow with the statistical significance of this result rules out a whole series of cosmological models at the $> 95\%$ confidence level (Feldman & Watkins 1994; Strauss et al. 1995); the LP result is in disagreement with all viable models at present.

The LP sample extended to $15\,000\text{ km s}^{-1}$, with an effective depth of $\sim 8000\text{ km s}^{-1}$. Therefore, the logical next step was to compare the LP result with peculiar velocities as found from applying the Tully-Fisher and FP methods to galaxies extending further out than any previous peculiar velocity studies. From Tully-Fisher studies of field and cluster spiral galaxies within 8000 km s^{-1} , Giovanelli et al. (1996, 1998a, 1998b) concluded that these galaxies do not show any evidence of such a bulk flow.

In order to investigate the reality of large-scale streaming motion on scales of up to 150 Mpc, we have studied the peculiar motions of 179 early-type galaxies in three directions of the South Equatorial Strip, at distances out to $\sim 20\,000\text{ km s}^{-1}$. We have obtained new and independent measurements of the peculiar velocity field of elliptical field galaxies at a depth similar to that of LP, using a combination of photometric and spectroscopic data. For further details of the project, see Müller (1997); the results for peculiar motions are analysed in Müller et al. (1998).

In this paper we present the spectroscopic data used in our study of the large-scale motions. From the spectra, galaxy redshifts were measured, and central velocity dispersions were obtained – the accurate determination of these is essential for the FP to be applied as a distance indicator. This paper is organised as follows. Sample selection and observations are described in Sect. 2, the basic reduction of the spectra is covered in Sect. 3, and the radial velocities and central velocity dispersions are derived in Sect. 4. The applied corrections are discussed in Sect. 5, and the results are given in data tables in Sect. 6. In Sect. 7 the results are compared internally and with results from the literature.

2. Samples and observations

Sample galaxies were selected from the new Automatic Plate Measuring Facility (APM) South Equatorial Strip

Catalog, which was made available prior to publication (Raychaudhury & Lynden-Bell 2000). The South Equatorial Strip Catalog ($-17^\circ.5 < \delta < +2^\circ.5$) is an uncharted region in the velocity field, because previously no good galaxy catalog existed for this region, and consequently the peculiar motions of galaxies in this strip had never been mapped. Redshifts had been previously measured for only about 20 of the sample galaxies, and velocity dispersion data existed for only a few of the sample galaxies.

The sample consists of early-type galaxies in three selected directions: (1) 15h10–16h10; (2) 20h30–21h50; (3) 00h10–01h30. The first region is about 20° from the direction of the LP bulk flow, the second region is almost perpendicular to the first, and the third is on the opposite side of the sky from the first, close to the direction of the Perseus-Pisces region and the South Galactic Pole. The APM South Equatorial Strip Catalog has a magnitude limit of $b_j = 17.0$ mag, which corresponds to 15.05 mag in Kron-Cousins R . All candidate galaxies in the three regions were examined on the POSS plates and then on CCD images to verify the morphological type. The original intention was to observe all galaxies down to this magnitude limit. We have both photometric and spectroscopic data for 179 of these galaxies, which resulted in a sample of E/S0 galaxies virtually complete to $R = 14.0$. The completeness drops for fainter magnitudes; galaxies down to $R = 15.0$ are included. New observations were carried out for all 179 galaxies, so that the sample has a fully independent data set with homogeneous observations, uniform data reduction, and consistent measurement techniques for all the galaxies.

In addition to the galaxies in the three sample regions, a number of standard galaxies from previous studies were also observed, for comparison purposes, in order to confirm the accuracy of the spectroscopic parameters obtained in this work. Comparison galaxies were selected from the following samples in the literature: Davies et al. (1987); González (1993); McElroy (1995); and Jørgensen et al. (1995). Spectra were also obtained for a sample of 40 galaxies in the Coma cluster, which was used as the calibration cluster for the FP distance-indicator relation. Galaxies were chosen to be E/S0 using earlier studies (e.g. Lucey et al. 1991; Jørgensen et al. 1993), and most lie within about 0.5° of the point midway between NGC 4889 and NGC 4874.

Spectroscopic observations were done at the 2.4 m Hiltner telescope and the 1.3 m McGraw-Hill telescope of the Michigan-Dartmouth-M.I.T. (MDM) Observatory on Kitt Peak, Arizona, and also at the 4.4 m Multiple Mirror Telescope¹ (MMT) on Mount Hopkins, Arizona. Data were collected during a series of nine observing runs

¹ The Multiple Mirror Telescope Observatory is operated by the Harvard-Smithsonian Center for Astrophysics jointly with the University of Arizona.

Table 1. Details of spectroscopic observing runs

Run Code	Dates of Observations	Telescope	Wavelength Range (Å)	$\Delta\lambda$ (Å/pix)	Res (Å)	Res (km s ⁻¹)
S1	28/06/93 – 04/07/93	MDM 2.4 m	4290 – 6780	2.43	4.7	110
S2	16/06/94 – 21/06/94	MDM 2.4 m	4440 – 6730	2.24	3.9	93
S3	11/09/94 – 18/09/94	MDM 2.4 m	4675 – 7035	2.31	5.0	118
S4	25/09/94 – 27/09/94	MMT 4.4 m	5000 – 5970	0.81	1.6	40
S5	21/10/94 – 23/10/94	MDM 2.4 m	4295 – 7165	2.81	5.6	133
S6	09/03/95 – 14/03/95	MDM 2.4 m	4305 – 6540	2.19	4.4	103
S7	29/05/95	MDM 1.3 m	4000 – 7100	3.04	5.6	132
S8	05/06/95 – 11/06/95	MDM 2.4 m	4320 – 6565	2.20	4.3	102
S9	01/09/95 – 04/09/95	MDM 2.4 m	4320 – 6565	2.20	4.3	102

Table 2. CCD and instrument parameters for spectroscopy

Parameter	Run Code			
	S1, S2, S3, S6, S8, S9	S4	S5	S7
Telescope	MDM 2.4 m	MMT 4.4 m	MDM 2.4 m	MDM 1.3 m
Spectrograph	Mark III	Red Channel	Mark III	Mark III
Grating/grism (<i>l</i> /mm)	grism (600)	grating (1200)	grism (600)	grism (600)
Blaze (Å)	5800	5750	5800	4600
Slit width (arcsec)	1.68	1.00	1.68	2.17
Detector	Tek CCD	Loral CCD	Loral CCD	Loral CCD
Format	1024 × 1024	800 × 1200	2048 × 2048	2048 × 2048
Binning	1 × 1	2 × 1	2 × 2	2 × 2
Readout Noise (e ⁻)	6.0	7.0	5.4	5.4
Gain (e ⁻ /ADU)	3.45	2.60	1.94	1.94
Pixel size (μm)	24	15	30	30
Spatial scale (arcsec/pixel)	0.777	0.300	0.971	1.794

between June 1993 and September 1995. Over 260 galaxy spectra were obtained. In total, 38 nights were allocated for this project, and 25 of them were usable. The main details of the observing runs are summarized in Table 1. (The resolution in Å given in Table 1 is the instrumental resolution, found from the FWHM of arc lines, whereas the resolution in km s⁻¹ is the spectrograph resolution or instrumental dispersion.) The spectral range was chosen to cover the Mgb band (around $\lambda_0 = 5177$ Å), the E-band (5270 Å) and the Fe I line (5335 Å). For some runs the H β (4861 Å) and Na D (5895 Å) features were also included. All observations were made with a long slit and a CCD detector. The setup and instrument parameters for all runs are shown in Table 2.

All observations on the two telescopes at MDM were made with f/7.5 and using the Mark III spectrograph, which consists of a grism, glass optics, and a CCD detector. Two different detectors were used with the MDM telescopes: the Tektronix TK1024A 1024² CCD, which is a thinned, back-illuminated CCD with a pixel size of 24 μm, and the Loral 2048² CCD, which is a thick, front-illuminated CCD with a 15 μm pixel size. Both CCDs are good cosmetically and have low readout noise. For the observations at the MMT we used the Red Channel: a spectrograph consisting of a collimator, a folding flat, a grating, and a CCD detector. The spectrograph was used in the high-throughput long-slit mode with a slit 180 arcsec long. The detector used at the MMT was a Loral 800 × 1200 CCD binned by 2 pixels in the narrower spatial

Table 3. Radial velocity standard stars and template stars

Star	Spectral Type	S/N per Å	Radial Velocity (km s ⁻¹)
HD 4388	K3 III	62	-28.3
HD 12029	K2 III	350	+38.6
HD 20893	K3 III	110	+5.9
HD 22072	DG7	120	+12.2
HD 36003	K0	106	-58.2
HD 38751	G8 III	220	+15.7
HD 51440	K2 III	117	+27.1
HD 64606	G5	137	+93.8
HD 65934	K0	130	+35.0
HD 72324	G9 III	68	+75.2
HD 73665	K0 III	120	+36.9
HD 74377	K0	84	-25.4
HD 90861	K2 III	140	+36.3
HD 132737	K0 III	110	-24.1
HD 165195	G5	50	-0.2
HD 171232	G8 III	142	-35.9
HD 172401	-	102	-73.0
HD 194071	G8 III	127	-9.8
HD 213947	K4 III	280	+16.7
HD 223094	K5 III	375	+19.6

direction (perpendicular to the dispersion). The CCD is very good cosmetically, with only a few traps.

The slit was usually oriented with the long axis running North-South. The instrumental resolution FWHM (in pixels and in Å) was determined by fitting a Gaussian to measure the widths of lines in calibration lamp spectra and of night-sky lines. Each galaxy was observed with a sufficiently long exposure time to ensure a high enough signal-to-noise ratio ($S/N \sim 20$) to enable the central velocity dispersion, as well as the redshift of the galaxy, to be determined accurately from the spectrum. At the MDM 2.4 m telescope, the average integration time needed was 2400 s; the integration times for individual galaxies ranged from 900 s to 2×3600 s according to the magnitude and surface brightness of the galaxy and the observing conditions. At the MMT, the average integration time per galaxy was 1200 s. A total of 263 spectra were obtained, of 238 galaxies. For some sample galaxies, more than one spectrum was obtained; an observation was repeated in some cases to provide a way to check the accuracy. Spectra were also obtained for KPNO IIDS spectrophotometric flux standard stars (Strom 1979), for use in flux calibration of the spectra. The exposure time was usually 360 s, and one flux standard star was observed per night.

In addition, several stars with known radial velocities were observed during each run. (Values of radial velocity for the standard stars were taken from Wilson 1953; Evans 1970; Abt & Biggs 1972; and Barbier-Brossat & Petit 1987.) These radial velocity standard stars were chosen to be of luminosity class III and in the range of spectral types G5 – K5. Most were K giants fainter than 7th magnitude. The observed stars are listed in Table 3. The same set of stars served as spectral templates for the determination of the velocity dispersions of the galaxies and as radial velocity standards for finding the galaxy redshifts. All the standard stars were trailed up and down the slit so that the slit illumination would be uniform and more similar to that of a galaxy. The exposure time was normally 420 s, which usually resulted in a very high S/N ratio.

Before and after the spectrum of each galaxy or standard star, a comparison spectrum was taken for use during wavelength calibrations. At MDM, Hg + Ne and Ne lamps were exposed for 0.2 s, and at the MMT He + Ne + Cu + Ar lamps were exposed for 120 s. Each night a series of bias frames was taken, as well as spectral flat field frames using an internal continuum flat lamp. Exposure times for flat fields were 30 s at MDM and 2 s at the MMT.

3. Preliminary data reduction procedures

Packages in the image processing system IRAF² (Tody 1986) were used for the basic reduction of the spectra. The main preliminary reduction steps, which are described in more detail below, are the following: (i) bias subtraction and dividing the data by a flat field; (ii) mapping the wavelength as a function of row and column by using the comparison exposures; (iii) subtracting the sky spectrum; (iv) removing the cosmic-ray hits from the spectra; and (v) extracting one-dimensional spectra from a sum over the aperture.

The bias level for each frame was found from the over-scan region. The bias frames were averaged and the residual bias level subtracted pixel-by-pixel from each image. From dark frames with exposures of 2400 s, a level always much less than one count was found. Since the dark current is flat, no dark count corrections were made. The flat field frames were combined to their median value, by using `noao.imred.ccdred.flatcombine`. This result was then normalized by fitting a cubic spline to the continuum in the wavelength direction and dividing the flat field by this fit to obtain the response function. The rms variation in the resulting flattened response frames was typically less than 0.5%. Each galaxy or star spectral frame was then divided by the response function.

² IRAF is distributed by National Optical Astronomy Observatories, which is operated by the Association of Universities for Research in Astronomy, Inc., under cooperative agreement with the National Science Foundation, U.S.A.

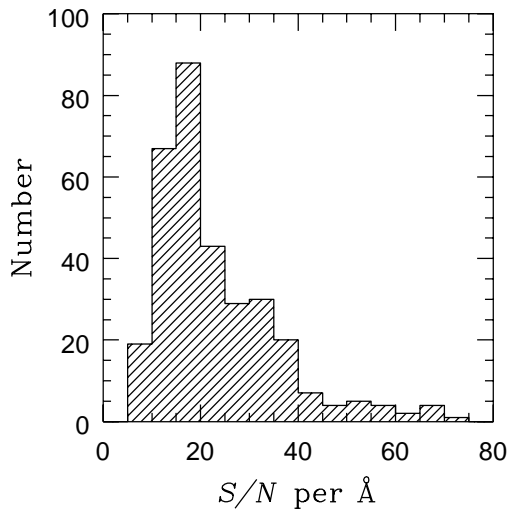


Fig. 1. The distribution of spectra as a function of the mean S/N per \AA measured at the wavelength of Mgb

The next step was to transform from pixel coordinates to a two-dimensional spatial scale with wavelength coordinates along the dispersion axis of the CCD image. Tasks in the package `noao.twodspec.longslit` were used for this. By means of 25 – 50 identified arc lines in the comparison lamp spectra, a polynomial was fitted to the wavelength solution, with an rms residual in the coordinate fit of 0.1 – 0.2 \AA . The two-dimensional spectra of stars and galaxies were calibrated in wavelength using the comparison lamp spectra observed before and after each object, and thus transformed to a linear wavelength scale.

The sky was fitted interactively using `background`, with the sky level found from unoccupied regions of the slit, and the sky background was subtracted. This worked well, since the galaxy occupied a relatively small part of the slit. Cosmic rays were removed by rejection using `images.lineclean`, with care being taken that absorption lines were unaffected. The final one-dimensional spectra were extracted by summing over an aperture covering the entire visible galaxy. This included tracing the mapping of the slit position across the CCD as a function of row or column. The package `kpnoslit.apall` was used interactively to fit the traced positions of the apertures. For all runs the trace was found to vary by at most 4 pixels across the CCD, in 1023 pixels. The typical width of the galaxy spectrum was about 20 pixels, so the maximum misalignment resulting from the tilt of the spectrum would be 0.1 pixels.

The summed one-dimensional spectra typically have 1000 – 20 000 counts at 5200 \AA , near the wavelength of Mgb. The mean value of the S/N per \AA was found for each spectrum, of galaxies and standard stars. The S/N was calculated from the mean number of photon counts in the spectrum in the wavelength range of the continuum bands of the Mgb spectral feature, also including in the

noise the contribution of the readout noise and the effect of subtracting the sky spectrum. For most spectra the resulting value of S/N per \AA is in the range of 15 – 40. A histogram of the frequency distribution of all the spectra with respect to S/N is shown in Fig. 1. The mean S/N for all spectra is 23.0. For sample galaxies it is 21.4, for Coma galaxies 27.3, and for standard galaxies 26.8. The S/N of a typical stellar observation is 100 – 200, which means that the stellar spectra can be considered to be noiseless.

At this stage the one-dimensional extracted spectra were inspected. Usually the sky subtraction was reasonably accurate, but the spectra were checked for night-sky emission lines, particularly those of [O I] at 5577 \AA and Hg at 5461 \AA , and if necessary these lines were removed by hand in cases of imperfect sky subtraction. There were sometimes cosmic rays which had not been removed completely, and these were also removed by hand. Three of the observed galaxies had spectra which were found to contain strong emission lines, and these galaxies were removed from the sample.

4. Determination of redshifts and velocity dispersions

The accurate determination of the line-of-sight central velocity dispersions of the galaxies is critical to FP analysis. A number of different methods exist for determining the velocity dispersion σ and the radial velocity cz . These include the Fourier quotient method (Sargent et al. 1977), the Fourier cross-correlation method (Tonry & Davis 1979), the Fourier difference method (Dressler 1979), and the Fourier fitting method (Franx et al. 1989).

For this study we used the Fourier cross-correlation method, as implemented in the IRAF package `rv.fxcor` which is based on the method of Tonry & Davis (1979). The spectra of the galaxy and the stellar template are cross-correlated in Fourier space, and the resultant maximum peak is fitted by a smooth symmetric function. The width and pixel shift of the peak are measures of σ and the galaxy redshift (in km s^{-1}), found by comparison with the known radial velocity of the template. An indicator of the accuracy of the resulting value of σ is the r value (Tonry & Davis 1979).

All spectra were rebinned, using `onedspec.dispcor`, to linear logarithmic wavelength coordinates. Total flux was conserved, and the same dispersion parameters were used for all spectra from all runs, resulting in spectra with logarithmic wavelength bins of $\Delta \ln \lambda = 6.46 \cdot 10^{-5}$. A cubic spline was fitted to the continuum for all spectra (template stars as well as galaxies). This fit was subtracted from the spectrum to flatten it; the resulting spectrum has zero mean in the continuum. The spectra were then Fourier filtered before the correlation. Data points outside the selected sample region were zeroed, and the ends of the region (12.5% on each end of the spectrum) were apodized with a cosine bell. A ramp function was used as

the filter. The parameters of the filter were adjusted to find the best combination. After the galaxy and template spectra had been thus prepared, the two sets of spectra were cross-correlated. In most cases the best region for cross-correlation was found to be 4900 – 5800 Å. This choice excludes the H β and Na D lines.

The galaxy spectra were Fourier cross-correlated in `fxcor` against each standard star in turn. The observed FWHM of the cross-correlation peak was transformed into a value for σ by direct calibration with broadened template spectra, using the procedure outlined by Baggley (1996). The spectrum of each template star was convolved with Gaussians of various known widths in the range 0 – 700 km s $^{-1}$, and the resulting broadened spectra were run in `fxcor` (with the same parameters) against the original template spectrum, giving the FWHM of the cross-correlation peak in each case. A calibration curve of this FWHM width versus the broadening σ for Gaussians of different widths was produced for each template star observation, by linear interpolation between the FWHM values from `fxcor`. The galaxy FWHM values were then converted into values for σ for the galaxy by reading off the calibration for that particular template star. An example of a calibration curve is shown in Fig. 2, for HD 194071, observed during run S8. In this case the resolution was approximately 100 km s $^{-1}$, and it can be seen from the figure that below this value of σ it is more difficult to find an accurate determination of velocity dispersion.

For every galaxy there is a set of different values for σ and cz , each pair of values the result of running the galaxy against a different stellar template spectrum. The values obtained by Fourier cross-correlation show small systematic differences depending on which stellar template is used. Template stars from all runs were used, a total of 45 observations of 20 different stars (as listed in Table 3). The rms difference between the estimates for cz and σ from different template stars was typically < 1% in cz and \sim 4% in σ .

In Fig. 3 the mean r value from the cross-correlation analysis of a spectrum is shown plotted against the S/N of that spectrum. From this plot it can be seen that the scatter is larger than would be expected if the S/N were the only factor affecting the r value. It could be that r is also sensitive to a mismatch between the features of the galaxy and those of some of the template spectra. Dalle Ore et al. (1991) found no systematic variation of the width of the cross-correlation curve with spectral type, and showed that errors in the velocity dispersion owing to spectral type mismatch are negligibly small. Jørgensen et al. (1995) found that template stars of the spectral type G8 – K3 result in significantly better fits than stars of types K4 – K5. For our sample data, we do not find this to be true in general. For a particular galaxy, certain templates work better than others, but we find that the best set of templates is different for each galaxy. We therefore combined the results for the velocity dispersion for each

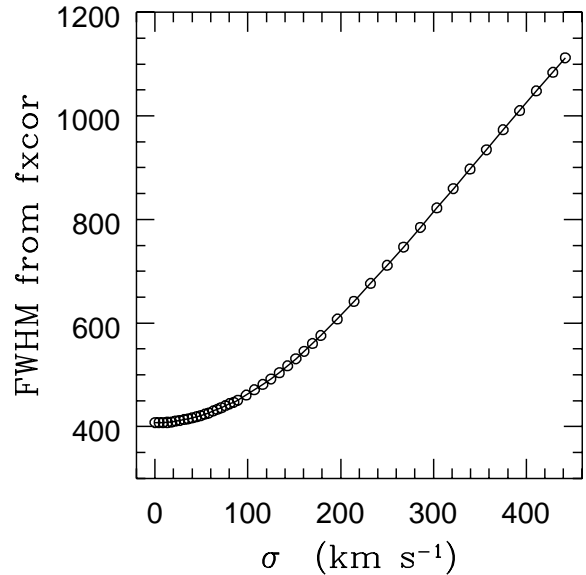


Fig. 2. The calibration curve for an observation of the standard star HD 194071. The points represent the FWHM from `fxcor` for the broadened template spectra compared with the unbroadened original template spectrum. The curve is found from linear interpolation between the points

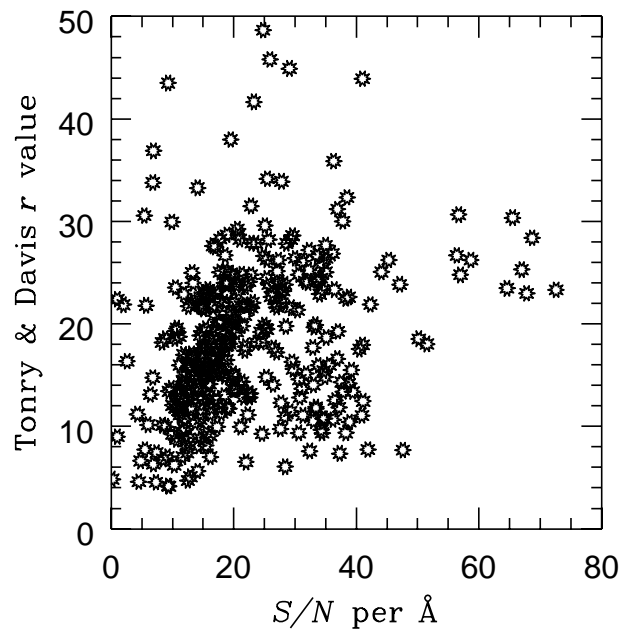


Fig. 3. A comparison of the S/N per Å of the spectra with the value of the Tonry & Davis r parameter from the cross-correlation, which is a measure of the ratio between the the peak height and the noise, and is therefore an indicator of the accuracy of the results

galaxy in such a way as to minimize the effect of the template mismatch problem. First, the mean of all the results from different templates was taken. Then the 2σ outliers were excluded and the mean was taken again, to give the final result. The redshift for each galaxy was estimated by calculating the mean observed heliocentric velocity from all the templates. For both σ and cz , the standard deviations from the means were calculated.

To check the zero-point for the redshift determinations, the spectrum of each radial velocity standard star was cross-correlated with the spectra of all the other standard stars, resulting in estimates of relative velocity. The radial velocity standards were run against each other in `fxcor` using the same scripts with the same parameters as used for the galaxies. For each star the mean of the estimates of heliocentric redshift was found, and compared with the known value of radial velocity for that star. The rms difference between the mean estimated value and the known value was about 20 km s^{-1} , which is therefore the accuracy of the zero-point of the radial velocities we determined.

Since a variation was observed among the separate determinations from each of the template spectra, estimates of the systematic errors for both redshift and velocity dispersion have been obtained from the rms scatter of the results from different templates. These error estimates are listed together with the results in Tables 5, 6, and 7.

5. Corrections to redshifts and velocity dispersions

5.1. Heliocentric correction to redshifts

Redshifts were corrected for the radial velocity of the template star and also corrected to the heliocentric system to take into account the motion of the Earth relative to the observed galaxy and the template star. This correction is included in `fxcor`; the result in the heliocentric frame is denoted v_{hel} .

5.2. Aperture correction to velocity dispersions

In E and S0 galaxies there are radial gradients in the velocity dispersion, with a higher velocity dispersion in the center of the galaxy than in the outer regions (Davies & Birkinshaw 1988; Franx et al. 1989; Davies et al. 1993). For this reason the derived “central” velocity dispersion parameter depends on the distance of the galaxy and on the size of the aperture used for the observation of the spectrum. It is therefore necessary to apply an aperture correction to transform the observed parameters so that they are independent of distance and of the telescope used.

The measured value of velocity dispersion depends on the velocity dispersion profile in the galaxy. Since the profile is not known for each galaxy, a general form must

be assumed. Jørgensen et al. (1995) established an aperture correction from kinematic models based on the available literature data. They used the models to derive the equivalent circular aperture for each rectangular aperture, and adopted a power law as the aperture correction to σ . The radius r_{ap} (in arcsec) of the equivalent circular aperture is found from $r_{\text{ap}} = 1.025\sqrt{wl/\pi}$, where w and l are the width and length of a rectangular aperture (slit). Jørgensen et al. (1995) correct the velocity dispersion to an aperture with a standard physical size, and use a value for the normalising aperture size of $2 r_{\text{norm}} = 1.19 h^{-1} \text{ kpc}$ ($h \equiv H_0/100 \text{ km s}^{-1} \text{ Mpc}^{-1}$.) This means that the velocity dispersion values are normalized to a velocity dispersion measured with an aperture of diameter $1.19 h^{-1} \text{ kpc}$, which is equivalent to 3.4 arcsec for a galaxy at the distance of the Coma cluster.

Baggley (1996) has shown that it is necessary to also take the effective radius r_e into account in the aperture correction, since the observed velocity dispersion of a galaxy depends on r_e as well. For two galaxies of different sizes at the same distance observed through the same aperture, the slit will cover more of the smaller galaxy and a different part of the galaxy profile will therefore be sampled; this dependence of σ on r_e must be removed to ensure that the velocity dispersion is truly a distance-independent quantity. We used Baggley’s formula for the aperture correction; it is a generalisation of the formula of Jørgensen et al. (1995) to take r_e into account:

$$\log \frac{\sigma_{\text{cor}}}{\sigma_{\text{obs}}} = 0.038 \log \left(\frac{r_{\text{ap}}}{r_{\text{norm}}} \frac{cz_{\text{gal}}}{cz_{\text{Coma}}} \frac{r_e^{\text{norm}}}{r_e^{\text{gal}}} \right), \quad (1)$$

where: σ_{obs} is the value of the velocity dispersion found from observation through an aperture equivalent to r_{ap} ; σ_{cor} is the velocity dispersion value corrected to the adopted normalising aperture size r_{norm} ; cz_{gal} is the redshift of the galaxy; cz_{Coma} is the redshift of the Coma cluster; r_e^{gal} is the effective radius of the galaxy; and r_e^{norm} is the normalising effective radius, which is taken to be 20 arcsec, following Baggley (1996) – this is the mean r_e of the galaxies in the sample of Jørgensen et al. (1995), which was used to derive the correction. This means that there will be no aperture correction for a galaxy with $r_e = 20$ arcsec, at the distance of the Coma cluster, observed through an aperture with an equivalent radius of 1.7 arcsec.

Equation (1) was used to calculate the corrections. The slit widths in the various instrumental setups are as shown in Table 2. For the length of the slit in the aperture, what is important is the extent of the galaxy along the slit, i.e. the length from which the one-dimensional spectrum was extracted; the spectrum was extracted out to the point where the luminosity had fallen to 10% of its peak value. The r_e value for each galaxy was taken from the results of the fitting and seeing-correction programs applied to the photometric data, as described in Müller (1997) and Müller et al. (1999). The value of the heliocentric redshift

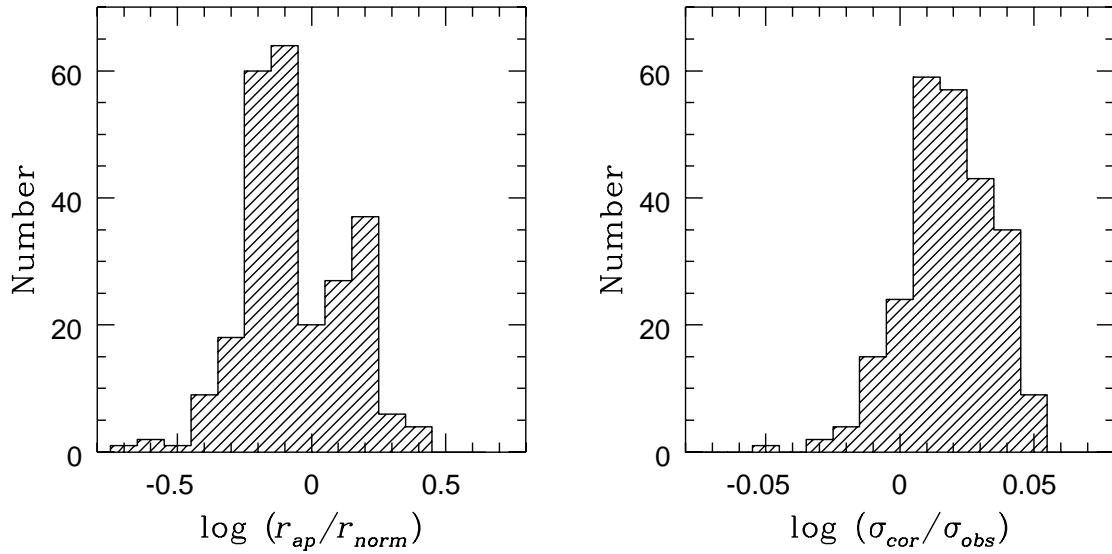


Fig. 4. Histograms for the galaxies in the three sample regions and in the Coma cluster. *Left:* A histogram of the aperture sizes of the sample galaxies relative to the normalising aperture radius, with r_{ap} in units of kpc at the distance (redshift) of the galaxy, and $2 r_{norm} = 1.19 h^{-1}$ kpc, equivalent to 3.4 arcsec for a galaxy at the distance of the Coma cluster ($h = 1$ was used). *Right:* A histogram of the sizes of the aperture corrections applied to the sample galaxies; σ_{obs} is the raw observed value and σ_{cor} is the aperture-corrected value of the velocity dispersion

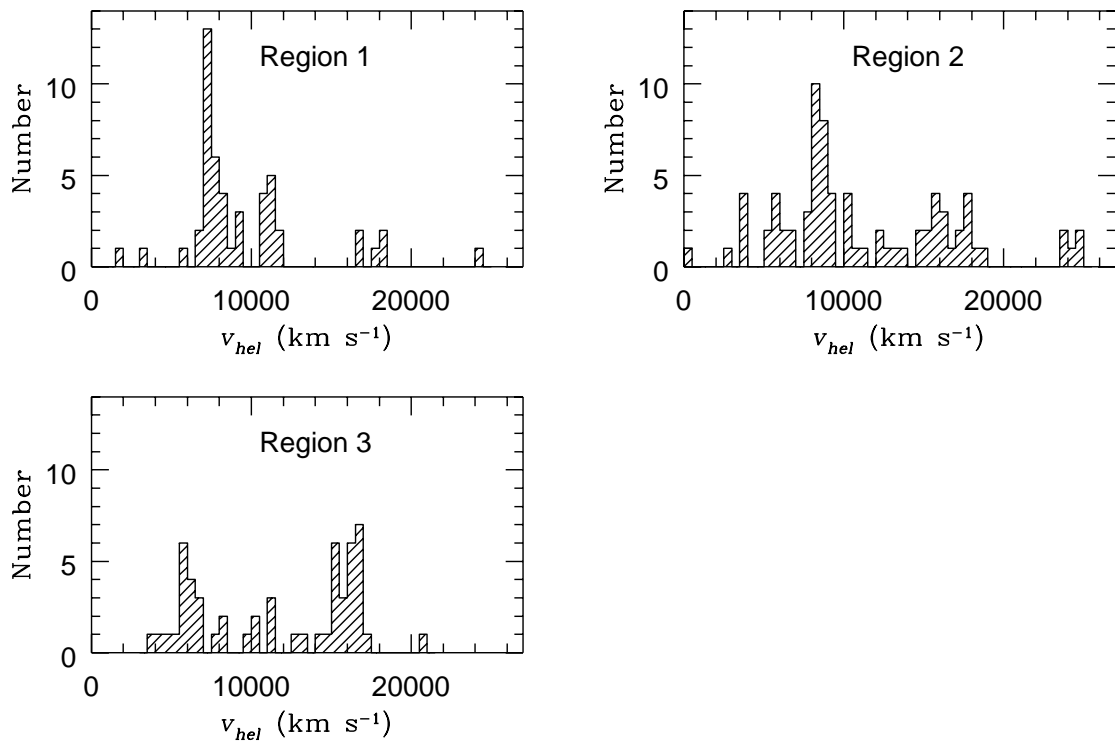


Fig. 5. Histograms of heliocentric radial velocity for observed galaxies in the three sample regions. Bin width 500 km s^{-1}

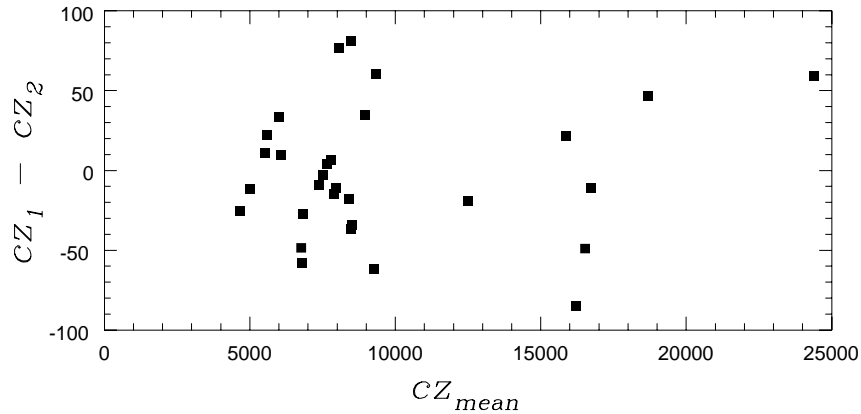


Fig. 6. Comparison of results for heliocentric radial velocity values determined from repeat observations

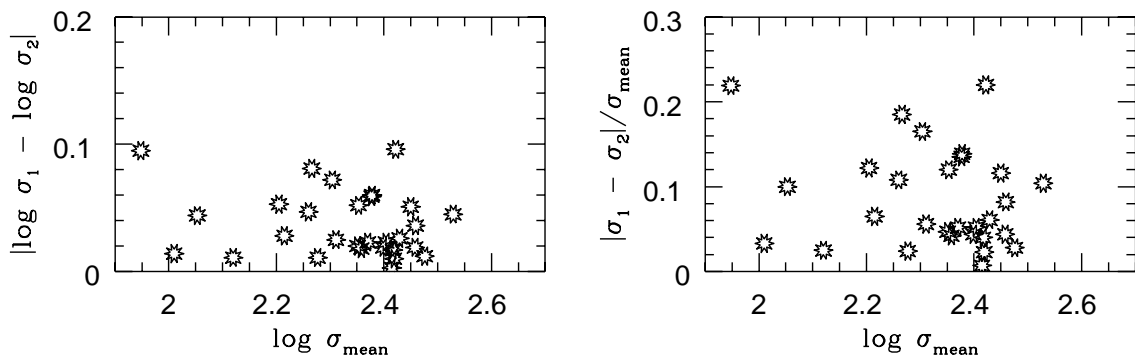


Fig. 7. Comparison of results for velocity dispersions measured from repeat observations

cz_{Coma} was taken to be 6917 km s^{-1} (Zabludoff et al. 1993), and $h = 1$ was used in the conversion of km s^{-1} to kpc.

The contribution to the aperture correction from the effect of r_e is more important than those for different slit sizes and different galaxy distances. From Eq. (1) it can be seen that the correction is negative for large or nearby objects (this is the case for the standard galaxies) and positive for galaxies with r_e less than 20 arcsec, which are smaller than or more distant than a 20 arcsec galaxy at the distance of Coma. The histogram of the applied aperture corrections in Fig. 4 shows that for the sample galaxies the correction is positive in most cases.

6. Results

6.1. Quality ratings for spectroscopic parameters

A quality rating was assigned to the results from each spectrum, on the basis of the cross-correlation results, and also after visual inspections of the spectra. Quality ratings were made as follows: $Q = 1$ for excellent spectra (S/N per $\text{\AA} > 20$; mean $S/N \sim 30$); $Q = 2$ for good spectra (mean $S/N \sim 16$); $Q = 3$ for acceptable spectra (mean

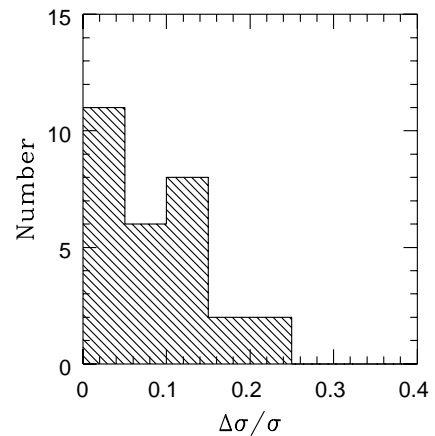


Fig. 9. Histogram of the fractional errors in the values of σ determined from repeat observations

$S/N \sim 11$); and $Q = 4$ for poor spectra ($S/N < 10$; mean $S/N \sim 4$). The mean Tonry & Davis r values for the four quality ratings are ~ 23 , ~ 17 , ~ 13 , and ~ 7 for ratings of $Q_{\text{spec}} = 1, 2, 3$, and 4 respectively. The percentage distribution of the quality ratings is shown in Table 4.

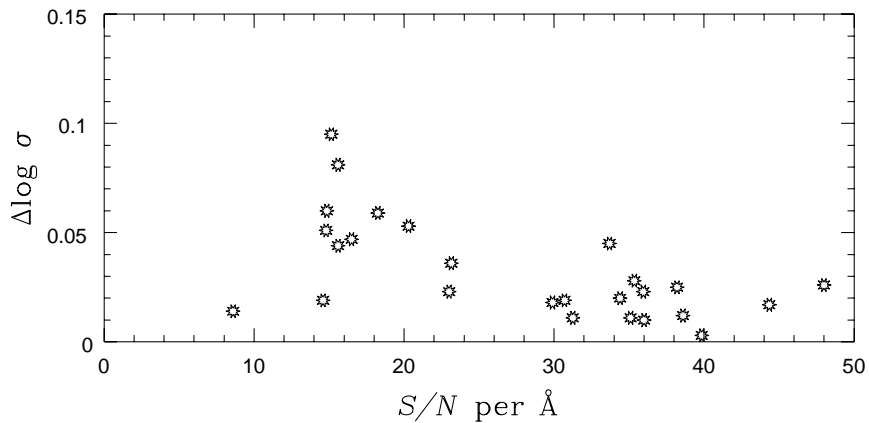


Fig. 8. The difference between results for velocity dispersions measured from repeat observations, plotted against the mean S/N per \AA of each pair of spectra

Table 4. Percentage distribution of quality ratings

Quality Rating	Percentage of Sample Galaxies				
	Standard galaxies	Region 1	Region 2	Region 3	Coma galaxies
$Q_{\text{spec}} = 1$	72	24	62	63	43
$Q_{\text{spec}} = 2$	28	26	26	28	32
$Q_{\text{spec}} = 3$	0	46	10	9	25
$Q_{\text{spec}} = 4$	0	4	1	0	0

For the spectra in the three sample regions, 78% of the spectra are of quality 1 or 2.

The S/N required to obtain a good measurement of radial velocity is lower than the S/N required to obtain a reliable velocity dispersion. For the galaxies with $Q = 4$ the signal was not strong enough to enable a reliable determination of the velocity dispersion. This was the case for galaxies of low surface brightness for which it was difficult to obtain spectra with a high enough S/N ratio. From these weak spectra, only redshifts were found, and these galaxies were not included in the sample used for distance determination. Below a certain limit, the values of velocity dispersion are less reliable. In the final sample we used only galaxies with high enough σ values to be determined accurately. The lower limit on usable σ values depends on the instrumental resolution. For the spectra taken at MDM, with a dispersion of $\sim 2.3 \text{ \AA/pix}$ and an instrumental resolution of $\sim 130 \text{ km s}^{-1}$, only velocity dispersions which are larger than 130 km s^{-1} can be measured reliably. For the spectra from the MMT, for which the dispersion was $\sim 0.80 \text{ \AA/pix}$ and the instrumental resolution was $\sim 40 \text{ km s}^{-1}$, the limit is lower.

6.2. Results for spectroscopic parameters

The results for the spectroscopic parameters are presented in Tables 5, 6, and 7. In cases where there were two or more spectra of the same galaxy available, the results with the smallest errors, from the spectrum with the highest S/N , were used. Histograms of the redshift distributions in the three sample regions are plotted in Fig. 5.

Spectroscopic results for the sample galaxies are given in Table 5. The columns in the table are as follows:

1. Galaxy number in the APM catalog (or the galaxy name from the NGC or CGCG catalog in a few cases); the first three digits of the APM galaxy number are the UK Schmidt plate number.
- 2 & 3. Right Ascension and Declination (epoch J1950.0) taken from the APM catalog.
- 4 & 5. Magnitude b_J (in mag) and major-axis diameter d (in arcmin) from the APM catalog (both values corrected for Galactic extinction). Preliminary values prior to final calibrations.
6. Heliocentric redshift v_{hel} (in km s^{-1}).
7. Estimated internal error in v_{hel} (in km s^{-1}).
8. Central velocity dispersion σ (in km s^{-1}).

Table 5. Spectroscopic parameters for the sample galaxies

Galaxy	Right Ascension	Declination	b_J	d	v_{hel}	err_v	σ	err_σ	Q_{spec}
Region 1									
87101144	16 01 52.14	-01 59 05.0	13.9	1.3	9259	26	305	4	1
65301306	15 16 17.18	-15 48 54.6	14.3	1.2	7296	17	270	16	1
65300653	15 24 14.86	-12 48 29.1	14.3	1.2	7351	15	232	21	1
72501710	15 17 51.60	-08 21 00.2	14.4	1.3	7573	22	149	18	3
79800188	15 47 10.58	-07 19 44.2	14.4	1.3	8032	28	208	3	1
65301588	15 12 23.45	-14 25 57.7	14.5	1.1	7419	18	286	5	3
65301596	15 12 14.43	-14 23 39.5	14.5	1.0	7475	18	168	9	1
87001759	15 36 17.64	-01 34 19.3	14.6	1.3	3439	4	154	3	1
65401564	15 41 57.11	-15 18 30.0	14.8	1.1	7320	19	209	15	1
72700354	16 07 48.41	-11 43 45.9	14.8	0.9	7964	17	109	25	3
79800136	15 48 02.65	-07 24 36.0	14.9	0.8	7742	10	231	13	3
87101109E	16 01 53.82	-01 36 41.8	-	-	9069	21	313	1	2
65402690	15 34 32.77	-16 25 59.2	15.0	1.0	7196	18	291	19	1
CGCG2158	15 13 02.87	+02 25 56.5	15.0	0.6	1849	22	63	17	1
72601433	15 31 40.06	-08 44 21.2	15.0	0.8	7129	17	265	13	1
79701386	15 20 15.85	-07 09 10.5	15.1	1.2	11730	17	239	5	2
65402668	15 34 40.55	-16 25 36.1	15.1	0.7	6798	12	147	13	1
79702357	15 12 55.64	-05 35 58.1	15.1	1.2	11404	29	228	2	2
79801072	15 30 47.53	-04 55 45.2	15.1	0.7	8000	15	171	11	3
87000696	15 44 59.18	-01 23 30.8	15.1	0.7	8972	20	276	17	2
65401595	15 41 43.20	-15 15 44.8	15.1	0.8	7439	14	175	9	2
79700187	15 29 43.12	-06 35 46.2	15.2	0.9	11112	8	240	8	3
65403060	15 31 44.41	-16 27 53.1	15.2	1.1	7403	15	106	8	3
65300973	15 20 29.81	-15 49 34.3	15.3	0.8	7109	19	130	7	3
65501546	15 58 50.53	-15 22 19.0	15.3	0.9	7510	11	171	10	3
65402909	15 32 54.07	-16 37 02.4	15.3	0.9	6849	13	142	15	3
87002300	15 30 24.64	+00 36 31.6	15.3	0.8	10980	18	248	17	3
65401438	15 42 48.68	-16 52 32.8	15.4	0.8	11342	28	249	11	2
65300169	15 29 48.37	-17 26 03.3	15.4	0.7	7050	6	131	8	1
65401086	15 45 06.95	-13 14 13.8	15.4	0.9	11275	13	184	14	3
65402811	15 33 40.66	-16 06 32.6	15.5	0.6	7855	10	206	8	2
72600774	15 40 56.84	-08 59 11.0	15.5	0.6	17737	22	316	9	3
87002308	15 30 19.55	+00 38 12.6	15.6	0.7	11781	22	323	15	2
79901311	15 57 33.40	-06 46 40.9	15.6	0.7	9146	18	98	12	3
79800922	15 33 30.16	-05 11 58.9	15.6	0.6	7077	28	127	5	3
65301134	15 18 21.41	-13 31 45.3	15.6	0.6	7263	13	163	15	2
72502368	15 12 33.13	-12 13 26.2	15.7	0.7	7634	36	82	4	3
65502352	15 52 05.13	-17 10 43.8	15.7	0.9	16533	11	229	12	3
65402361	15 36 32.47	-16 32 16.3	15.7	0.6	10505	31	232	8	2
72502210	15 13 49.98	-08 49 51.2	15.7	0.7	5600	13	16	16	3
87001111	15 41 10.37	-01 35 46.1	15.8	0.6	16897	20	223	6	3
72600488	15 44 54.15	-11 43 03.4	15.8	0.7	24012	51	397	62	3
87100850	16 04 28.03	-01 41 33.1	15.9	0.7	10839	10	132	22	3
79702517	15 11 38.51	-04 14 50.8	15.9	0.8	10978	23	413	11	2
79800965	15 32 46.84	-03 19 02.3	15.9	0.5	18012	19	303	8	3
65502359	15 52 07.79	-15 13 22.9	15.9	0.6	17513	44	-	-	4
87002295	15 30 27.12	+01 08 12.7	16.1	0.6	15068	30	-	-	4
86902718	15 10 28.74	+02 12 43.1	16.1	0.5	11391	32	177	22	3
72801203	16 17 51.62	-10 20 59.9	14.6	1.1	8472	29	215	4	2
72801189	16 17 57.70	-09 46 17.2	14.9	0.9	8006	24	209	2	2

Table 5. continued

Galaxy	Right Ascension	Declination	b_J	d	v_{hel}	err_v	σ	err_σ	Q_{spec}	
Region 2										
NGC 7010	21 01 55.45	-12 32 17.1	14.3	1.9	8480	19	228	3	1	
81405781	20 53 56.12	-04 01 20.4	14.7	1.1	6025	10	156	10	1	
81303405	20 35 10.59	-06 16 00.6	15.1	1.0	3844	5	89	5	1	
81502978	21 17 38.08	-05 05 20.4	15.1	0.9	9102	17	367	9	3	
67200327	21 44 53.58	-13 24 53.2	15.1	0.8	5418	13	167	14	1	
81303115	20 36 22.29	-05 08 59.3	15.2	1.2	3797	10	131	19	1	
74402521	21 48 16.53	-09 30 02.4	15.2	0.9	5380	20	213	15	1	
67003337	20 52 46.63	-13 39 34.8	15.3	0.9	24515	38	555	7	3	
66901323	20 39 01.84	-14 01 30.9	15.4	0.8	8409	18	265	2	1	
81603636	21 33 27.73	-03 33 44.1	15.4	0.8	8027	14	257	11	3	
74402642	21 46 50.74	-10 05 44.3	15.5	1.1	23869	10	598	14	2	
81405745	20 53 59.57	-03 32 27.4	15.5	0.6	5979	11	126	14	1	
67001814	21 00 46.20	-15 10 30.3	15.5	1.1	8455	16	241	13	1	
81503740	21 14 12.52	-04 42 24.4	15.6	0.8	13765	11	266	22	1	
67003179	20 53 39.80	-14 35 43.1	15.6	0.8	8468	6	139	3	2	
81601185	21 45 01.36	-06 35 43.1	15.6	0.9	6103	15	153	13	1	
81602395	21 39 15.52	-06 56 13.7	15.6	0.8	6906	20	158	6	2	
81404709	20 56 46.08	-04 38 08.9	15.7	0.8	4680	49	-	-	4	
67003696	20 50 48.81	-14 41 58.9	15.7	0.8	7580	11	178	6	1	
81602330	21 39 29.90	-04 26 37.3	15.7	0.7	8225	25	114	8	1	
67102806	21 27 46.38	-16 20 28.2	15.7	0.7	9353	7	215	4	1	
74400983	21 41 10.20	-08 18 11.9	15.7	0.9	15305	22	351	4	1	
81404583	20 57 05.76	-02 50 34.2	15.8	0.8	17209	34	510	16	2	
74401483	21 35 55.30	-08 07 58.1	15.8	0.9	15751	7	348	3	2	
67201749	21 37 30.96	-14 27 30.1	15.8	0.6	18358	25	514	13	1	
67202822	21 38 18.48	-16 55 16.6	15.8	0.7	15509	29	469	13	1	
67103161	21 20 15.95	-16 11 58.7	15.8	0.7	13294	19	231	4	1	
67202363	21 47 30.24	-17 24 35.4	15.8	0.6	10185	10	174	14	1	
74300882	21 15 30.52	-07 32 02.2	15.8	0.7	8270	10	122	18	2	
67001913	21 00 17.18	-16 59 57.9	15.9	0.6	8716	17	246	1	2	
81603664	21 33 17.98	-03 22 20.5	15.9	0.6	2873	4	104	3	1	
81301006	20 46 07.02	-07 10 50.8	15.9	0.7	12441	17	162	15	1	
67001942	21 00 05.85	-16 00 34.5	15.9	0.7	8501	27	341	7	1	
81602522	21 38 30.84	-04 31 25.2	15.9	0.8	16219	11	268	14	1	
81302133	20 40 42.55	-04 40 54.1	16.0	0.7	8611	19	140	13	3	
74301907	21 19 33.98	-09 38 45.1	16.0	0.7	12340	14	297	11	1	
74200901	21 05 07.05	-10 36 38.4	16.0	0.7	8780	19	213	5	1	
74405800	21 34 26.16	-11 27 24.7	16.0	0.7	17794	21	266	11	1	
81601843	21 41 57.89	-06 23 11.7	16.0	0.8	15768	31	249	1	3	
81601806	21 42 05.59	-07 17 17.9	16.0	0.7	5998	9	121	15	2	
67002128	20 59 13.51	-13 22 13.3	16.0	0.7	8492	17	197	9	2	
81501871	21 22 42.66	-03 19 32.6	16.0	0.6	5640	20	77	15	2	
81601380	21 44 05.41	-05 27 38.9	16.0	0.7	6584	15	92	11	1	
74200951	21 04 47.84	-10 55 06.0	16.0	0.7	8269	10	141	12	2	
81504194	21 12 07.77	-02 33 55.1	16.1	0.7	7957	7	111	3	2	
67002172	20 58 59.41	-13 30 36.4	16.1	0.7	8822	19	254	7	1	
81603573	21 33 47.15	-04 11 51.4	16.1	0.6	15726	30	195	2	2	
81602191	21 40 10.46	-07 05 52.5	16.1	0.6	16043	33	321	1	2	
74401426	21 36 27.77	-07 31 39.3	16.1	0.7	10425	21	49	24	2	
81602252	21 39 51.84	-06 39 24.5	16.2	0.6	10348	30	134	6	2	

Table 5. continued

Galaxy	Right Ascension	Declination	b_J	d	v_{hel}	err_v	σ	err_σ	Q_{spec}	
81600601	21 47 54.17	-05 36 33.7	16.2	0.6	16715	17	325	19	2	
67003806	20 50 17.86	-16 31 30.7	16.2	0.6	12891	21	330	5	1	
81602134	21 40 27.29	-07 17 52.8	16.2	0.6	15015	31	251	2	2	
74202489	20 55 31.78	-07 57 12.4	16.2	0.8	23717	30	349	6	3	
67201815	21 36 19.16	-14 35 25.1	16.3	0.6	17930	23	446	16	2	
67201810	21 36 28.63	-14 32 41.1	16.3	0.5	17972	16	286	2	2	
81600354	21 49 07.77	-03 13 57.5	16.4	0.6	16461	17	228	13	1	
74404851	21 45 19.53	-12 08 59.7	16.4	0.7	14761	22	175	7	1	
81304119	20 31 56.30	-06 40 17.5	16.4	0.6	24394	37	360	11	1	
67001459	21 02 45.64	-12 34 59.3	16.4	0.5	7940	16	128	10	1	
67001377	21 03 14.05	-16 00 59.9	16.4	0.6	8511	19	134	8	1	
67002239	20 58 37.77	-13 17 52.6	16.4	0.6	9258	12	167	49	1	
74302893	21 21 43.60	-11 44 05.5	16.4	0.6	9011	20	133	12	1	
81405246	20 55 21.94	-04 41 41.1	16.4	0.5	24804	50	452	18	1	
74402668	21 46 34.70	-09 51 06.0	16.4	0.8	10281	37	315	11	1	
74402837	21 44 20.85	-10 44 57.8	16.4	0.5	10820	14	193	8	1	
81400846	21 08 17.34	-03 58 52.3	16.4	0.5	9427	5	317	9	1	
74400638	21 44 34.04	-08 37 23.9	16.4	0.6	17950	22	259	17	1	
67102743	21 28 57.59	-16 18 04.8	16.4	0.5	18655	17	320	15	1	
67201875	21 34 48.75	-14 55 07.4	16.4	0.5	11424	17	297	34	1	
81406413	20 52 10.94	-03 31 43.4	16.4	0.5	5823	17	51	15	1	
66900782	20 44 16.43	-14 09 03.1	16.4	0.6	8742	4	110	9	1	
67100128	21 29 20.05	-13 59 28.8	16.4	0.6	17408	13	322	17	1	
88920974	21 53 26.20	-01 45 11.9	-	1.0	8045	17	323	14	1	
88520340	20 44 50.30	+00 06 58.1	-	2.0	3804	16	172	15	1	
88720594	21 11 23.79	+02 21 24.1	-	1.9	14544	37	154	10	3	
88520337	20 44 36.89	+00 10 41.1	-	0.7	3865	7	41	31	3	
Region 3										
68100721	00 41 02.46	-08 27 37.1	14.4	1.2	5960	20	142	14	1	
60800316	00 28 18.95	-12 59 46.4	15.0	0.9	6137	21	73	24	1	
68101448	00 32 08.14	-11 02 30.3	15.0	0.8	6210	18	154	13	1	
68001213	00 15 02.00	-09 49 15.6	15.1	1.0	6718	23	169	7	1	
68101358	00 33 27.93	-10 23 49.2	15.1	0.8	5982	14	195	12	1	
68101582	00 30 00.82	-12 20 25.9	15.1	1.1	16971	5	155	5	2	
61100299	01 25 02.07	-13 59 59.2	15.2	1.0	9894	18	212	11	1	
68100166	00 48 45.71	-08 52 07.3	15.2	0.8	4282	15	168	11	1	
68301163	01 13 59.64	-08 14 26.4	15.2	0.7	5552	16	165	12	1	
61001080	01 06 22.24	-15 40 21.3	15.3	1.0	15911	15	263	21	1	
68001229	00 14 54.03	-09 48 27.0	15.3	1.1	6823	9	118	14	1	
68100890	00 39 18.72	-09 34 38.6	15.4	0.8	16690	24	354	10	2	
68101426	00 32 25.81	-09 37 03.4	15.4	0.7	6969	11	148	11	1	
68300617	01 22 47.56	-12 10 25.5	15.4	0.8	15021	28	257	15	1	
61001389	00 57 46.77	-15 34 06.1	15.4	0.9	16567	26	341	6	2	
68100622	00 42 27.48	-09 09 47.5	15.4	0.7	5804	3	203	21	3	
68101215	00 35 26.55	-08 20 55.3	15.5	0.9	11214	34	204	9	2	
60800542	00 26 07.72	-13 17 11.2	15.6	0.7	7778	12	223	12	1	
61002238	00 56 22.55	-16 44 20.3	15.6	0.8	16284	28	339	13	3	
68300547	01 23 55.82	-08 49 25.6	15.6	0.7	5253	13	87	11	2	
68201452	00 55 39.28	-08 29 15.7	15.6	1.1	4602	8	178	26	1	
61001909	01 06 21.72	-16 12 47.6	15.7	0.9	12597	21	345	8	2	
68101346	00 33 36.91	-07 58 26.3	15.7	0.6	11191	13	245	15	2	

Table 5. continued

Galaxy	Right Ascension	Declination	b_J	d	v_{hel}	err_v	σ	err_σ	Q_{spec}
60901605	00 31 47.85	-12 55 55.0	15.8	0.7	8030	16	265	13	1
61002004	01 03 47.71	-16 48 34.6	15.8	0.8	11242	29	276	18	1
61100351	01 23 38.67	-13 40 53.1	15.8	0.9	14201	26	326	3	2
68201703	00 53 20.82	-10 15 22.6	15.8	0.8	16356	9	209	12	2
60800452	00 27 00.10	-14 16 10.3	15.9	0.7	16200	14	203	14	2
68201935	00 51 05.05	-08 31 35.7	15.9	0.8	13297	28	275	4	1
68101515	00 31 01.35	-09 28 13.5	15.9	0.6	5543	17	31	23	2
68100388	00 45 20.77	-12 03 50.9	15.9	0.5	5886	14	87	6	1
68101166	00 36 02.25	-09 23 15.9	16.0	0.5	6094	20	44	21	1
68201775	00 52 43.24	-11 31 48.3	16.0	0.7	16375	20	273	13	1
68101270	00 34 38.49	-09 43 55.1	16.0	0.6	15877	18	141	18	3
68100879	00 39 21.80	-11 06 24.8	16.0	0.6	15860	19	199	3	1
61102514	01 16 52.44	-16 54 12.4	16.1	0.6	6061	8	110	13	2
68201336	00 57 07.98	-09 09 03.2	16.1	0.7	16614	23	213	15	1
61000670	00 53 34.10	-13 37 41.5	16.1	0.6	16804	26	408	6	1
61100750	01 14 38.10	-14 15 39.3	16.1	0.6	15411	29	304	13	1
68201473	00 55 25.46	-09 47 42.8	16.1	0.6	15060	23	210	17	1
68101018	00 37 47.50	-07 43 43.7	16.1	0.6	3692	5	6	6	1
61100580	01 18 30.28	-14 06 42.2	16.2	0.6	15384	7	349	18	1
68201394	00 56 21.84	-09 02 42.6	16.3	0.5	8055	7	133	13	1
68100760	00 40 38.46	-10 08 07.2	16.3	0.5	15142	7	220	5	3
68300512	01 24 25.53	-07 37 57.6	16.3	0.5	10191	32	344	3	1
61100364	01 23 19.43	-12 46 09.6	16.4	0.5	10262	24	218	3	1
61101581	01 18 08.13	-14 07 33.0	-	-	14708	3	246	12	1
61101582	01 18 06.14	-14 07 33.6	-	-	16458	10	236	18	1
61101583	01 17 52.50	-14 09 06.4	-	-	15292	19	224	8	1
61101584	01 17 52.46	-14 14 09.7	-	-	20954	5	326	11	1
61001081	01 06 29.38	-15 41 12.2	-	-	17451	28	454	10	2
61001082	01 06 21.22	-15 41 17.3	-	-	16530	29	170	13	2
61001084	01 06 25.64	-15 42 15.1	-	-	16913	12	228	8	2
61001085	01 06 33.34	-15 46 50.8	-	-	16300	10	158	17	3

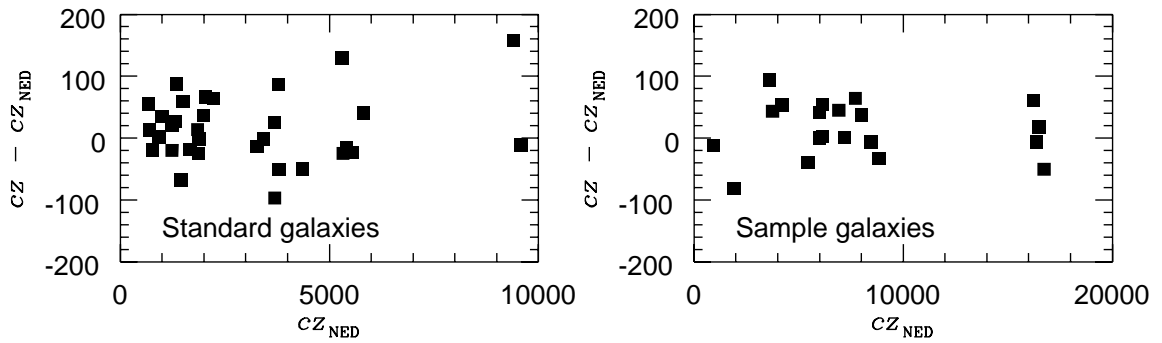


Fig. 10. Comparison of results for heliocentric radial velocity with published data for 32 standard galaxies and 20 sample galaxies

Table 6. Spectroscopic parameters for the standard galaxies

Galaxy	Right Ascension	Declination	v_{hel}	err_v	σ	err_σ	Q_{spec}
NGC 5831	15 01 34	+01 24 54	1648	19	139	3	1
NGC 5845	15 03 28	+01 49 36	1383	15	196	2	1
NGC 5846A	15 03 56	+01 47 12	1688	18	232	3	1
NGC 6020	15 55 00	+22 33 00	4307	16	173	15	1
NGC 6051	16 02 48	+24 03 54	9578	17	347	13	2
NGC 6086	16 10 36	+29 36 54	9549	25	313	15	1
NGC 7619	23 17 43	+07 56 00	3753	14	269	14	1
NGC 7626	23 18 10	+07 56 36	3431	15	313	8	1
NGC 227	00 43 03	-01 48 18	5434	16	243	15	1
IC 1696	01 22 19	-01 52 42	5860	11	166	8	2
NGC 533	01 22 57	+01 30 00	5521	13	224	20	1
NGC 636	01 36 36	-07 45 54	1861	19	155	3	1
NGC 7468	23 00 30	+16 20 00	2094	22	137	40	2
NGC 7751	23 44 24	+06 35 00	3247	10	123	3	2
NGC 541	01 23 12	-01 38 00	5401	20	186	14	1
NGC 545	01 23 24	-01 36 00	5296	18	203	14	2
NGC 1550	04 17 00	+02 18 00	3714	23	327	15	1
NGC 1587	04 28 06	+00 33 00	3597	22	239	16	1

9. Estimated internal error in σ (in km s^{-1}).

10. Quality rating Q_{spec} for the spectrum.

In Table 5, the galaxies are ordered by magnitude, with a few exceptions. The galaxies CGCG2158 (in Region 1) and NGC 7010 (in Region 2) were added for completeness. In Region 1, the galaxy denoted 87101109E is the elliptical galaxy close to 87101109, which was found to be a spiral. Also included are some galaxies from plates which are not in the final APM catalog: two galaxies from plate 728 in Region 1, and four galaxies (from plates 885, 887, and 889) in Region 2 (no magnitudes are given for these galaxies, since the magnitude zero-pointing and plate-matching calibration was not done for these plates). In Region 3, there are eight extra galaxies: a group near 61101581 and a group near 61101081, for which spectra had been obtained, and which were included in the sample.

The results for the spectroscopic parameters of the standard galaxies and Coma galaxies are presented in Tables 6 and 7 respectively. The columns are as in Table 5, except that magnitudes and major-axis diameters are not given. The names of the galaxies in Coma are taken from the Dressler numbers as catalogued by Dressler (1980).

7. Internal and external comparisons

7.1. Internal comparisons

The reliability of the determinations of the spectroscopic parameters was checked by comparing the results from re-

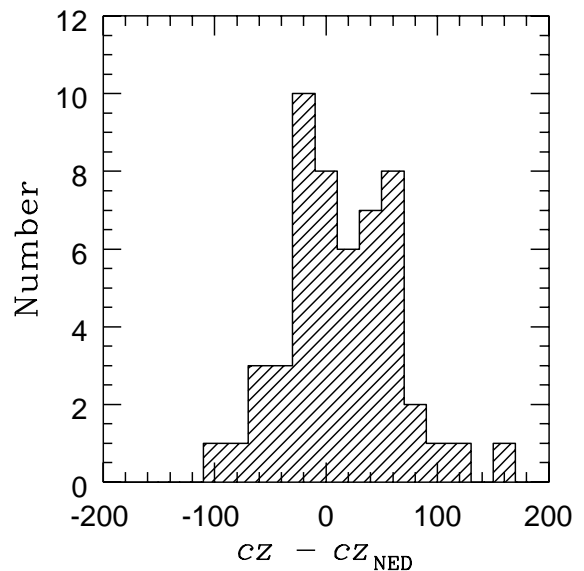


Fig. 11. Distribution of differences between measured redshifts and the redshifts given by NED (literature redshifts), for 52 standard galaxies and sample galaxies

peat observations of the same galaxy. There are 30 galaxies of which two spectra were obtained for each, and for these galaxies the differences in parameters were found.

Table 7. Spectroscopic parameters for the Coma galaxies

Galaxy	Right Ascension	Declination	v_{hel}	err_v	σ	err_σ	Q_{spec}
Coma 31	12 54 59.0	+27 46 00	7369	15	256	14	1
Coma 46	12 55 07.5	+27 52 55	6074	12	210	13	1
Coma 49	12 59 29.9	+27 53 36	7893	15	267	11	1
Coma 69	12 56 43.5	+28 03 16	7072	29	265	39	3
Coma 70	12 56 42.8	+28 02 21	6336	7	187	27	2
Coma 72	12 56 27.2	+28 03 33	5656	14	199	4	2
Coma 87	12 57 05.9	+28 03 45	7825	6	66	37	3
Coma 88	12 57 04.5	+28 07 09	6790	19	236	16	3
Coma 103	12 57 06.0	+28 09 13	4744	8	205	4	1
Coma 105	12 56 58.7	+28 10 59	5104	25	170	10	2
Coma 106	12 56 58.1	+28 10 05	5087	8	199	11	2
Coma 107	12 56 55.6	+28 09 25	6452	9	138	1	3
Coma 118	12 58 15.2	+28 11 42	7552	28	141	8	1
Coma 124	12 57 19.8	+28 11 02	6678	4	236	6	1
Coma 125	12 57 17.9	+28 11 47	6900	3	174	5	2
Coma 129	12 57 11.1	+28 13 53	7223	11	266	11	3
Coma 130	12 57 09.6	+28 13 09	7209	8	234	1	2
Coma 133	12 56 50.6	+28 14 33	4859	7	257	5	1
Coma 134	12 56 39.4	+28 13 51	6978	6	184	1	2
Coma 135	12 56 35.7	+28 14 23	8286	33	137	14	2
Coma 136	12 56 30.6	+28 14 12	5682	14	266	9	2
Coma 143	12 58 30.1	+28 16 42	4990	15	217	13	1
Coma 148	12 57 43.7	+28 14 54	6360	22	431	20	1
Coma 150	12 57 42.0	+28 16 33	7241	5	202	15	3
Coma 151	12 57 40.0	+28 15 32	6350	5	157	21	2
Coma 153	12 57 19.2	+28 15 57	6912	90	215	9	1
Coma 159	12 56 48.4	+28 14 54	6881	20	252	4	1
Coma 160	12 56 41.0	+28 15 58	7672	14	153	13	1
Coma 168	12 58 24.5	+28 21 40	7088	18	226	23	3
Coma 172	12 57 50.3	+28 18 45	5827	9	211	15	3
Coma 179	12 56 53.1	+28 21 13	4638	16	234	15	1
Coma 180	12 56 49.3	+28 20 53	7780	11	104	6	3
Coma 193	12 57 30.8	+28 24 00	7501	20	126	12	2
Coma 194	12 56 39.3	+28 23 47	7980	2	285	2	2
Coma 206	12 57 50.9	+28 28 17	8507	17	268	15	1
Coma 207	12 57 43.8	+28 26 31	6779	16	82	12	2
Coma 217	12 57 32.8	+28 31 08	6803	9	194	4	3
Coma 232	12 58 03.8	+28 36 55	6012	11	163	13	1
Coma 239	12 55 07.0	+28 44 28	6322	3	205	1	1
Coma 240	12 55 09.0	+28 45 06	6834	15	246	2	1

7.1.1. Redshifts

Internal comparisons of radial velocities are shown in Fig. 6 for 30 galaxies with two spectra each. The order (cz_1 and cz_2) in which the two results have been considered is arbitrary. The rms scatter is $\Delta cz_{\text{hel}} = 40.7 \text{ km s}^{-1}$ for the comparisons of repeat observations.

7.1.2. Velocity dispersions

In Fig. 7, internal comparisons of velocity dispersions are shown for 29 galaxies with two spectra each. An estimate of the accuracy is the rms scatter of $|\log \sigma_1 - \log \sigma_2|$, which

is 0.045. In Fig. 8, the errors in repeat measurements of σ are also shown as a function of S/N per Å. It is clear from the plot that the repeatability depends on the S/N of the spectrum. For a S/N of 40 – 50, velocity dispersions can be determined to within 4 – 5% (from $\Delta\sigma/\sigma$) and for a S/N of ~ 20 (which is the case for most of the galaxies in the sample) the accuracy is about 8 – 10%.

Figure 9 is a histogram of the fractional errors in σ for 29 repeat observations. The rms scatter in $\Delta\sigma/\sigma$ is 0.103, which means that σ can be determined to 10% accuracy. The galaxies for which there are repeat measurements are typical of those in the whole sample, so these estimated errors are representative of the true errors.

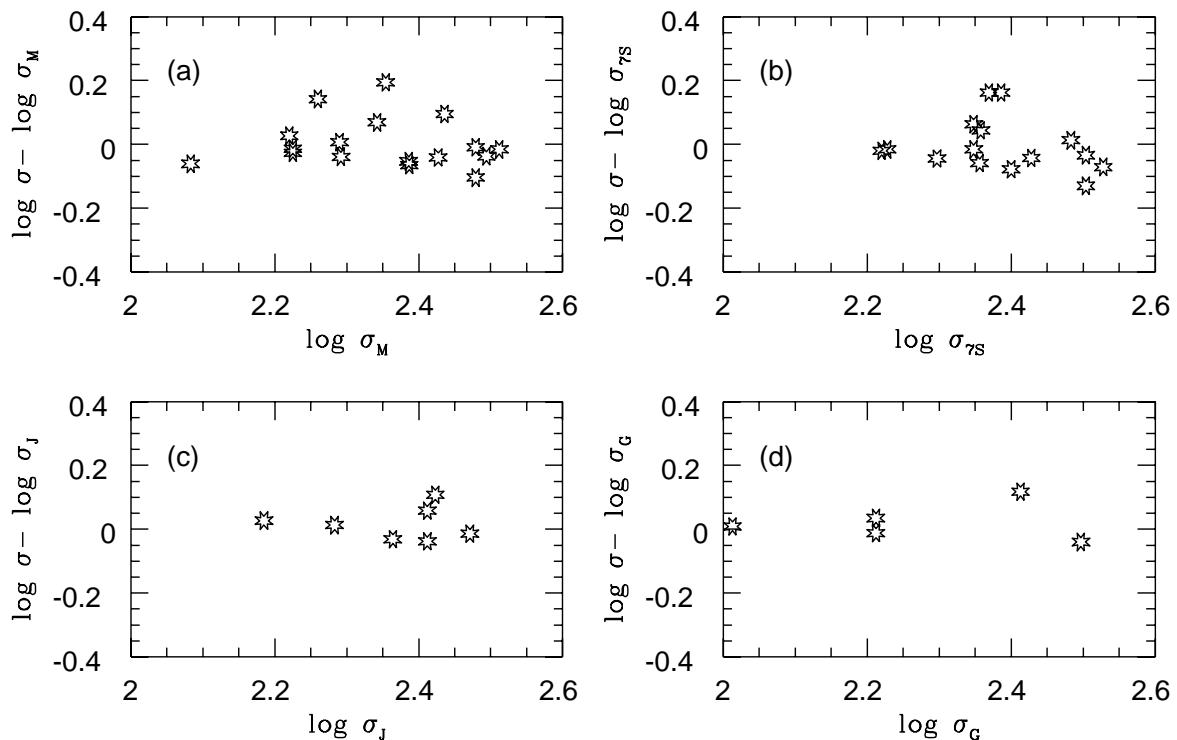


Fig. 12. Comparison of the results for velocity dispersions of standard galaxies with values from the literature: **a)** McElroy (1995); **b)** Davies et al. (1987); **c)** Jørgensen et al. (1995); **d)** González (1993)

7.2. External comparisons

7.2.1. Redshifts

Results for redshifts were compared with values from NED³ (Madore et al. 1992) and from the ZCAT compilation of redshifts (Huchra et al. 1992), and the differences were found to be relatively small. Redshift comparisons were possible for 32 standard galaxies and 20 sample galaxies. (Redshifts were available for only a small fraction of the galaxies in the sample regions, since the South Equatorial Strip had not been well studied before.)

The determinations of radial velocity for these two sets of galaxies were compared with redshifts from the literature, and the results are shown in Fig. 10. For both data sets the agreement is good. For all 52 galaxies for which literature redshifts were available, the distribution of differences between the measured redshifts and the literature values is shown in the histogram of Fig. 11. The values of the mean absolute difference $|cz - cz_{\text{NED}}|$ are 42.4 km s^{-1} and 37.3 km s^{-1} for the standard galaxy and sample galaxy comparisons respectively; the rms differences are 56.0 km s^{-1} and 45.8 km s^{-1} . This shows that the redshifts are of adequate reliability.

³ NED, the NASA/IPAC Extragalactic Database, is operated by the Jet Propulsion Laboratory, California Institute of Technology under contract with the National Aeronautics and Space Administration.

7.2.2. Velocity dispersions

In order to make sure that the values of velocity dispersions determined here are scaled to the standard system, the results for the velocity dispersions of standard galaxies were compared with published values. Our data set overlapped with the following sets: (i) the compilation of McElroy (1995) (17 galaxies in common); (ii) Davies et al. (1987) (7S) (15 galaxies in common); (iii) Jørgensen et al. (1995) (7 galaxies in common); and (iv) González (1993) (5 galaxies in common).

The data set of Davies et al. (the 7S data) defines a good standard system since it is frequently used for comparisons. The comparison with the results of Davies et al. is shown in Fig. 12 together with comparisons with data from the other sources. The difference between the values from this study and the literature data, $\Delta \log \sigma = \log \sigma(\text{this study}) - \log \sigma(\text{literature})$, are shown plotted against $\log \sigma(\text{literature})$. There do not appear to be any offsets or systematic differences relative to the velocity dispersions of the four data sets. The rms scatter of $\Delta \log \sigma$ is 0.066, 0.111, 0.036, and 0.021 for the plots in (a), (b), (c), and (d) respectively. The agreement is best for comparisons with González (1993) and Jørgensen et al. (1995), which are the most recent data sets, although the numbers of galaxies in common are smaller.

8. Summary

We have obtained new radial velocities and central velocity dispersions for 179 E and S0 galaxies in three selected directions in the APM South Equatorial Strip, as well as for 40 galaxies in the Coma cluster. Observations were made with the 2.4 m and 1.3 m telescopes of the MDM Observatory on Kitt Peak, Arizona, using the Mark III spectrograph, and at the 4.4 m MMT, using the Red Channel. The spectra have a mean S/N per Å of 23.

Radial velocities and central velocity dispersions have been determined by the Fourier cross-correlation method. The velocity dispersions have been corrected for the effect of the aperture size and for the galaxy's effective radius. We find that the typical uncertainties on the derived parameters are $\pm 40 \text{ km s}^{-1}$ in cz and ± 0.045 in $\log \sigma$. In comparisons with literature data, no offsets or systematic differences are seen. The accuracy of 8 – 10% in the derived velocity dispersions is high enough for the values to be used in the application of Fundamental Plane analysis. The results given here have been used together with photometric data (Müller et al. 2000) to derive Fundamental Plane distances to the sample galaxies in order to determine their peculiar velocities and thereby investigate the reality of large-scale streaming motion; results have been reported in Müller et al. (1998).

Acknowledgements. GW wishes to acknowledge partial support from the Alexander von Humboldt Foundation during a visit to the Ruhr-Universität Bochum, and also from NSF grant AST93-47714. KM acknowledges financial support from a Dartmouth Fellowship and from a Research Studentship at the European Southern Observatory in Munich.

References

- Abt H.A., Biggs E.S., 1972, *Bibliography of Stellar Radial Velocities* (KPNO). Latham Process Corp., New York
- Baggley G., 1996, Ph.D. Thesis, Oxford University
- Barbier-Brossat M., Petit M., 1987, *Catalogue Bibliographique de Vitesses Radiales Stellaires*
- Dalle Ore C., Faber S.M., González J.J., Stoughton R., 1991, *ApJ* 366, 38
- Davies R.L., Birkinshaw M., 1988, *ApJS* 68, 409
- Davies R.L., Burstein D., Dressler A., et al., 1987, *ApJS* 64, 581
- Davies R.L., Sadler E.M., Peletier R.F., 1993, *MNRAS* 262, 650
- Dressler A., 1979, *ApJ* 231, 659
- Dressler A., 1980, *ApJS* 42, 565
- Evans D.S., 1970, *Catalogue de Vitesses Radiales Stellaires Moyennes*, Observatoire de Marseille
- Feldman H.A., Watkins R., 1994, *ApJ* 430, L17
- Franx M., Illingworth G.D., Heckman T., 1989, *ApJ* 344, 613
- Giovanelli R., Haynes M.P., Wegner G., et al., 1996, *ApJ* 464, L99
- Giovanelli R., Haynes M.P., Freudling W., et al., 1998a, *ApJ* 505, L91
- Giovanelli R., Haynes M.P., Salzer J., et al., 1998b, *AJ* 116, 2632
- González J.J., 1993, Ph.D. Thesis, University of California at Santa Cruz
- Huchra J.P., Geller M.J., Clemens C., Tokarz S., Michel A., 1992, *Bull. CDS* 41, 31
- Jørgensen I., Franx M., Kjaergaard P., 1993, *ApJ* 411, 34
- Jørgensen I., Franx M., Kjaergaard P., 1995, *MNRAS* 276, 1341
- Kogut A., Lineweaver C., Smoot G.F., et al., 1993, *ApJ* 419, 1
- Lauer T.R., Postman M., 1994, *ApJ* 425, 418
- Lucey J.R., Bower R.G., Ellis R.S., 1991, *MNRAS* 249, 755
- Madore B.F., Helou G., Corwin Jr. H.G., et al., 1992, in: Worrall D.M., Biemesderfer C., Barnes J. (eds.) *Astronomical Data Analysis Software and Systems I*, ASP Conf. Ser. 25, Astron. Soc. Pac., San Francisco, p. 47
- McElroy D.B., 1995, *ApJS* 100, 105
- Müller K.R., 1997, Ph.D. Thesis, Dartmouth College
- Müller K.R., Freudling W., Watkins R., Wegner G., 1998, *ApJ* 507, L105
- Müller K.R., Freudling W., Wegner G., 2000 (in preparation)
- Raychaudhury S., Lynden-Bell D., 2000, *A Catalogue of Galaxies in the Southern Equatorial Strip*. Cambridge University Press, Cambridge UK
- Riess A.G., Press W.H., Kirschner R.P., 1995, *ApJ* 445, L91
- Sargent W.L.W., Schechter P.L., Boksenberg A., Shortridge K., 1977, *ApJ* 212, 326
- Scoddeggio M., Giovanelli R., Haynes M.P., 1997, *AJ* 113, 101
- Strauss M.A., Willick J.A., 1995, *Phys. Rep.* 261, 271
- Strauss M.A., Cen R.Y., Ostriker J.P., et al., 1995, *ApJ* 444, 507
- Strom K.M., 1979, *Standard Stars for Intensified Image Dissector Scanner Observations*, Kitt Peak National Observatory Booklet
- Tody D., 1986, *Proc. SPIE* 627, 733
- Tonry J.L., Davis M., 1979, *AJ* 84, 1511
- Wilson R.E., 1953, *General Catalogue of Stellar Radial Velocities*, Carnegie Institute of Washington Publication 601, Washington DC
- Zabludoff A.I., Huchra J.P., Geller M.J., 1993, *AJ* 105, 788